Mechanics of Materials 56 (2012) 11–22

Contents lists available at SciVerse ScienceDirect

Mechanics of Materials

journal homepage: www.elsevier.com/locate/mechmat

The respective influence of microstructural and thermal softening on adiabatic shear localization

S. Osovski [a,*], D. Rittel [a], A. Venkert [b]

[a] Faculty of Mechanical Engineering, Technion, 32000 Haifa, Israel
[b] Department of Physics, NRCN, Beer-Sheva 84190, Israel

ARTICLE INFO

Article history:
Received 18 May 2012
Received in revised form 11 September 2012
Available online 28 September 2012

Keywords:
Dynamic fracture
Microstructures
Thermomechanical process
Adiabatic shear localization
Finite elements

ABSTRACT

It has recently been shown that dynamic shear failure of crystalline solids can be initiated by local microstructural changes (dynamic recrystallization, DRX), instead of the commonly assumed thermal softening mechanism. We systematically investigate the respective contribution of thermal and microstructural softening to the initiation of dynamic shear localization, by means of a fully coupled numerical model incorporating the two softening mechanisms in an adjustable manner. Our results indicate that, for those materials that exhibit early DRX, (e.g. Ti6Al4V), the role of thermal softening is negligible, whereas for materials with late (e.g. pure Ti) or no DRX, thermal softening effects become dominant. The strength of the thermomechanical coupling term (thermal softening) is found to determine the local temperatures, with the strongest effect being achieved in the absence of coupling, together with the formation of thermal "hot spots". Thermal softening is found to regulate the evolution of the local temperature, in the sense that the softened material both stores and dissipates smaller increments of strain energy. The results of this study allow for a general classification of the material proneness to dynamic shear localization as a function of its thermo-physical characteristics.

1. Introduction

Since the early seminal contribution of Zener and Hollomon (1944), it has been commonly accepted that the main reason for adiabatic shear localization is the competition between strain hardening and thermal softening, as a result of thermomechanical coupling. Thermal softening is assumed to gradually reduce the strain-hardening capacity of a material to a point where it reaches a plateau, followed by a negative slope which is interpreted as the sign of instability. Based on this premise, a large body of analytical and numerical work has been dedicated to the subject. While an exhaustive list of references is beyond the scope of this paper, one should mention the book of Bai and Dodd (1992) which lists a wealth of experimental observations, and that of Wright (2002), which discusses extensively modeling aspects of the phenomenon. One should also mention the early work of Molinari and Clifton (1987) who modeled shear localization based on a geometrical perturbation approach. Note here that one could also study the effect of a thermal perturbation, and show that its growth may lead to instability. Such a perturbation would arise, for example, from "hot spots", namely local sharp gradients in temperature, that develop in the strained material as a result of a local thermomechanical heterogeneity. As of today, irrespective of the constitutive model that is adopted, a prevailing criterion for the onset of adiabatic shear localization is the attainment of a critical strain value. This parameter can also be viewed as a failure criterion for engineering design. It is important to note that such an approach marks the onset of the catastrophic failure, thereby lumping initiation and growth of the adiabatic shear band in one and single parameter.

* Corresponding author.
E-mail address: shmulo@gmail.com (S. Osovski).

0167-6636/$ - see front matter © 2012 Elsevier Ltd. All rights reserved.
http://dx.doi.org/10.1016/j.mechmat.2012.09.008

Recently, Medyanik et al. (2007) proposed a criterion for the onset of adiabatic shear bands (ASB) which was related to the appearance of DRX, by assuming a minimum temperature for its onset. Thereafter, the build-up of DRX is assumed to cause the material to behave like a viscous fluid, resulting in stress collapse. The approach used in this work, however, still requires elevated temperatures as a trigger for DRX and subsequent ASB, while this requirement stands in contradiction with some of the experimental observations reported by Rittel and Wang (2008).

Alternatively, Rittel et al. (2006, 2008) suggested to consider the dynamically stored energy of cold work (SECW) as a criterion for the *onset* of shear localization. This energy, once it reached a certain threshold, was suggested to lead to the formation of dynamically recrystallized grains (DRX), which may appear long before final failure, and whose effect was create soft enclaves in the surrounding hardening material. Final failure occurs therefore as a result of the growth and coalescence of islands of dynamically recrystallized phase, as shown by Osovski et al. (2012). In other words, these authors suggested that the onset of dynamic shear localization is primarily related to microstructural transformations which were indeed observed long before any significant self-heating of the material develops (Rittel et al., 2008). In this context, Schoenfeld and Kad (2002) modeled the dynamic mechanical response of Ti6Al4V using crystal plasticity concepts and a cell method. In their work, both slip and twinning were represented, contributing to different local flow stresses, depending on the cell orientation. In addition, the contribution of anisotropy to adiabatic shear band formation was explicitly addressed. One should also mention the work of Clayton (2009) who considered energy storage concepts and microstructural heterogeneity in aluminum alloys to model their dynamic performance. In this work, a coarse grained model of crystal plasticity was used, leading to the conclusion that the microstructure should be tailored to obtain optimal impact toughness of these materials. Stored energy considerations were applied as a criterion for the onset of dynamic shear localization was examined numerically by Dolinsky et al. (2010) and was shown to be successful for a variety of problems involving dynamic loading.

In a recent work, Osovski et al. (2012) compared their microstructural observations of annealed Ti6Al4V and commercially pure Ti which were impacted dynamically to pre-determined levels of strain. These authors observed that while Ti6Al4V exhibits early DRX at about half its failure strain (Rittel et al., 2008), pure Ti only shows DRX at the late stages of its deformation, close to 0.9 its failure strain. Moreover, while Ti6Al4V deforms essentially by *slip* (dislocation mediated plasticity), pure Ti exhibits massive *twinning* which precedes markedly the formation of DRX and immediate subsequent failure. These findings were rationalized in terms of strain energy storage, noting that twinning, which does not store significant amounts of energy (Padilla et al., 2007; Bever et al., 1973), acts therefore as a delaying factor for dynamic recrystallization. Osovski et al. (2012) modeled the interaction between slip-DRX-twinning using a finite element model for which each element represents a typical grain of the material. This model allowed for the characterization of the evolution of the DRX'ed phase whose continuity is interpreted as final failure. Moreover, since each of the three deformation micromechanisms stores energy in a different manner, local temperatures could be calculated at the grain level, revealing that the overall temperature rise remained quite modest throughout the deformation process while no localized hot elements (hot spots) were observed, in agreement with previous experimental work. Yet, this work did not consider the degradation of the mechanical properties with the increase of temperature, even modest, nor did it consider latent heat release associated with recrystallization.

Consequently, the dynamic shear localization process can be triggered by two softening mechanisms, one microstructural and the second thermal. However, very little is known on the respective contribution and importance of each mechanism to the overall failure process. Therefore, the following fundamental questions remain to be elucidated:

1. What is the precise contribution of thermal softening, if at all, with respect to the above-mentioned microstructural softening. In other words, is thermal softening alone, sufficient to trigger dynamic shear localization, and if not, when does it become significant?
2. What is the contribution of the enthalpy release which is associated with the recrystallization process? How does it affect the thermal balance, both globally and locally?
3. What is the contribution of hot spots, if any, to the onset of adiabatic shear failure?

This paper attempts to answer these questions through numerical modeling, based on suitable modifications of the model developed by Osovski et al. (2012), which did not address these aspects. Throughout this work, typical materials will be considered, whose thermomechanical and physical properties (detailed in the sequel) are selected such as to cover the cases of materials that exhibit DRX only (e.g. Ti6Al4V), mixed DRX and twinning (e.g. pure Ti), or no DRX (e.g. pure Ta).

The present paper is organized as follows: We first present in detail the numerical model, choice of internal variables and their physical meaning. Next we report the main results of the systematic simulations, to be discussed in the following section. This section is followed by a summary and conclusions, thus answering the questions posed above.

2. Micromechanical model

2.1. Physical assumptions underlying the micromechanical model

Following the experimental observations of Osovski et al. (2012), our model considers three possible deformation mechanisms responsible for the plastic flow: twinning (twin boundary formation), slip (dislocation motion), and a third mechanism referred to as DRX-mediated plasticity. Those three mechanisms are treated using a rule of mix-

ture to describe the mechanical, microstructural and thermal evolution of the material. In the following subsections, the assumptions made as to the contribution of each mechanism to the hardening behavior of the material as well as its contribution to energy storage and dissipation, will be discussed. Here, it is important to state that in the context of this work, the meaning of a micromechanical study is to be understood as a heuristic, experimentally-driven approach.

2.1.1. Hardening behavior

- Dislocation mediated plasticity – the volume fraction of the material which undergoes slip, is assumed to obey a parabolic hardening law.
- Twinning – the formation of new twin boundaries is considered to contribute to the hardening by acting as obstacles for dislocation motion, and as such is treated using a Hall-Petch like term (Eq. (1c)). However, unlike in the commonly used Hall-Petch relation, the exponent is chosen to be unity instead of one half, thus implying that dislocation pile-ups against a twin boundary cannot activate a dislocation source (Remy, 1978).
- DRX-mediated plasticity – the nano-grained DRX'ed fraction of the material is assumed to behave as an ideally plastic similar, as shown in experimental observations carried out on ultra-fine-grained materials (Jia et al., 2001), and as discussed by Bouaziz et al. (2010).

Moreover, twin formation is assumed to stop in a given element once DRX formation starts in this element. Twinning, which complements dislocation activity, is no longer necessary once DRX provides its own additional contribution to the deformation process.

2.1.2. Energy balance and physical considerations

- Dislocation mediated plasticity – it is commonly admitted that dislocation activity is the main energy storage mechanism when discussing the SECW. To calculate the amount of SECW due to dislocation activity and the amount of energy dissipated as heat, the Quinney–Taylor coefficient (Taylor and Quinney, 1934) was utilized for the volume fraction of material involved in slip.
- Twinning – following the work of Padilla et al. (2007), it was assumed that all of the energy resulting from twin mediated plasticity is fully dissipated, and as such only contributes to heat generation and temperature increase in the adiabatic process.
- DRX-mediated plasticity – the DRX'ed fraction of the element is assumed not to store energy at all. Furthermore, as will be discussed later, the formation of a DRX'ed grain, namely the increase in DRX volume fraction, is a process involving the release of stored energy (latent heat) which was the driving force for its creation.
- DRX evolution – since there is no experimental data as to the evolution of the volume fraction of DRX with ongoing deformation, it was assumed that the volume fraction of DRX is evolving according to the Johnson–Mehl–Avrami–Kolmogorov (JMAK) equation Avrami, 1939, as a function of the stored energy. The JMAK equation, which is often used to describe phase transitions in the solid phase, implies that the formation of DRX is an accelerating process whereby initially, DRX'ed grains appears gradually, and as their number increases, the whole process of DRX formation accelerates.
- It is important to note, that all the quantities related to energy that will be presented in the following sections are specific quantities, and as such are influenced by the change in volume fraction and not by the volume itself.

2.2. Hardening and evolution equations

The viscoplastic response of the material (ignoring thermal effects) was modeled using an overstress viscoplastic formulation as shown in Equation set (1), below:

$$\dot{\varepsilon}^p = \dot{\varepsilon}^0 \left[\frac{\sigma_{flow}}{g(\varepsilon^p)}\right]^{1/n} \tag{1a}$$

$$g(\varepsilon^p) = (1 - f_{drx})\sigma_y^0 + f_{drx}\sigma^{drx} + (1 - f_{drx} - f_{twins})R(x, \varepsilon_m) \tag{1b}$$

$$R(x, \varepsilon_m) = K_t\left(\frac{1}{x}\right) + K_d(\varepsilon_m)^m \tag{1c}$$

with $g(\varepsilon^p)$ being a rate-independent yield surface. The first term in $g(\varepsilon^p)$refers to the yield stress of the (tested) coarse-grained Titanium, while σ^{drx} in the second term is to be understood as the flow stress at which DRX first appears (upon reaching the energetic threshold). Each of the above mentioned stresses is multiplied by its relative volume fraction (f_{drx}, f_{twins}). The third term in Eq. (1b) is an isotropic hardening term $R(x, \varepsilon_m)$ which consists of two parts (Eq. (1c)). The contribution of evolving density of twins acting as barriers for dislocation motion enters the equation as a Hall-Petch like term, where K_t is a hardening constant and x is the average distance between twins given by $x = 2t(1 - f_{twins})/f_{twins}$ with t being the average twin width. The second hardening term in Eq. (1c) is the hardening term resulting from dislocation activity during deformation with K_d being the hardening constant, and ε_m being the strain in the non-twinned regions, defined through Eq. (2). Finally, the rate dependence of the flow stress is given by the Eq. (1a). Here, $\dot{\varepsilon}^p$ is the plastic strain rate, ε^p being the plastic strain and n is a rate-sensitivity constant, while $\dot{\varepsilon}^0$is a reference strain rate. The total plastic strain is divided into strain coming from an increase in twin volume fraction, and strain arising from dislocation motion and DRX. The total plastic strain increment is thus given by:

$$d\varepsilon_p = (1 - f_{twins})d\varepsilon_m + \varepsilon_T df_{twins} \tag{2}$$

where ε_T is the strain due to twinning which is taken to be the shear strain of the active twinning system (γ_T) divided by the Taylor factor. The evolution equations for the twin and DRX volume fractions, as well as the stored energy, are given in Equation set (3).

$$f_{twins} = \begin{cases} \frac{1}{N}[\arctan(2\pi a\varepsilon_p - 2\pi b) - \arctan(-2\pi b)]; & U < U_{drx} \\ Const. & U \geqslant U_{drx} \end{cases} \tag{3a}$$

$$f_{drx} = \begin{cases} 0 & U < U_{drx} \\ 1 - \exp\left(-k_{drx}\left(\frac{U-U_{drx}}{U_{drx}}\right)^{n_{drx}}\right) & U \geqslant U_{drx} \end{cases} \tag{3b}$$

$$U(\varepsilon_p) = (1 - f_{drx} - f_{twins})(1-\beta)\int_0^{\varepsilon_p} \sigma_{flow} d\varepsilon_p \tag{3c}$$

with U being the stored energy of cold work, U_{drx} – the threshold energy for the onset of the recrystallization process Here, a, b, and N are fitted to reproduce the average number of twins per grain measured at different strains, while k_{drx}, n_{drx} are rate constants in the Johnson–Mehl–Avrami–Kolmogorov equation, and β is the assumed Taylor Quinney coefficient of the phase undergoing slip.

2.3. Temperature rise and thermal softening effects

By assuming adiabatic conditions and using equation set (4), with ρ being the density and C_p the specific heat capacity, the local temperature rise, in the absence of DRX, can be calculated *on an element basis*.

$$\left.\begin{aligned} W - U &= \int \sigma_{flow} d\varepsilon_p - U = Q \\ \Delta T &= \tfrac{Q}{\rho C_p} \end{aligned}\right\} \tag{4}$$

To account for the temperature rise resulting from latent heat release during a recrystallization event, the formation enthalpy (H_f) is considered to be a fraction ($0 \leqslant f_{lh} \leqslant 1$)of the critical energy for DRX, with 0 meaning that no enthalpy is released and 1 meaning that all of the stored energy is being released. Since H_f is a specific energy, it has to be multiplied by the volume fraction of the material being recrystallized (df_{drx}), so that the corresponding local temperature rise is given by Eq. (5):

$$\left.\begin{aligned} \Delta H_f &= f_{lh}(df_{drx} U_{drx}) \\ \Delta T &= \tfrac{Q+\Delta H_f}{\rho C_p} \end{aligned}\right\} \tag{5}$$

In the following sections of this work we will use this parameter (f_{lh}) to investigate the effect the latent heat release might have on the shear localization process, a comparison will be presented between a case in which all of the stored energy is released at each increment of the volume fraction of DRX, and a model which does not take this latent heat into account.

The temperature rise inside the element is then used to study the effects of thermal softening, assuming a linear dependence (α) of the mechanical properties on the temperature.

Therefore, thermal effects were inserted into the model through five physical parameters using the same thermal softening coefficient as shown in Equation set (6):

$$\begin{pmatrix} E(T) \\ K_t(T) \\ K_d(T) \\ \sigma_y^0(T) \\ \sigma_{drx}(T) \end{pmatrix} = \begin{pmatrix} E(T_0) \\ K_t(T_0) \\ K_d(T_0) \\ \sigma_y^0(T_0) \\ \sigma_{drx}(T_0) \end{pmatrix} (1 - \alpha\Delta T) \tag{6}$$

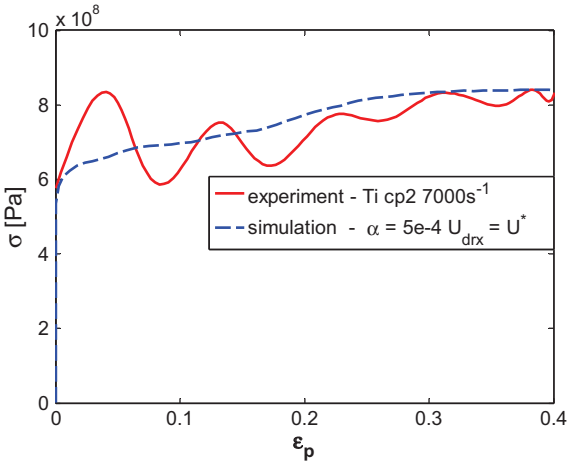

Fig. 1. A comparison between the experimentally obtained stress–strain curve and a simulation using the parameter set given in Table 1.

Table 1
Model parameters.

Property	Value	Source
E	116 GPa	Literature Boyer et al. (1994)
v	0.3	Idem
U^*	92 (MPa/m^3)	Estimated based on experimental observations
m	0.25	Assumed
K_t	$1.8e-3 (MPa\,m)$	Fitted to measured stress–strain curve
K_d	$215 (MPa)$	Fitted to measured stress–strain curve
β of the slip phase	0.6	Assumed
σ_y^0	500 (MPa)	Measured
γ_T	0.174	Literature Hosford (2005)
Taylor factor	2.5–3.15 (evenly distributed)	Assumption based on values commonly used in literature
t – twin thickness	2 (μm)	Measured
a	5	Fitted to reproduce the average number of twins per grain measured at different strains
b	1	Idem
N	7.4594	Idem
k_{drx}	0.5	Fitted to produce failure at the experimentally observes strain
n_{drx}	8.7	Idem
$\dot{\varepsilon}^0$	1000 (1/s)	Assumed
n	0.0539	Obtained from experimental stress–strain curves at different strain rates
α	$0{:}1e-3$	Adjustable
f_{lh}	0:1	Adjustable

While the linear dependence on temperature as assumed in Eq. (6) is probably not the real material behavior, given the lack of accurate experimental data for each feature of the model, Eq. (6) was chosen to reflect a strong thermal softening mechanism.

However, the first term in Eq. (6) may be justified by looking at Hill and Shimmin's work (1961) on various metals including Titanium alloys, where it was found that Young's modulus actually decreases almost linearly with temperature. All the model parameters and constants, as well as the method for their determination are summarized in Table 1. Fig. 1 presents a comparison between the experimentally obtained stress–strain curve and the simulated one.

3. Numerical model

3.1. FEM model

The numerical (FEM) simulations were carried out using (ABAQUS\Explicit, 2009a) solver, into which our VUMAT user-subroutine was implemented to introduce the micro-mechanical thermo-viscoplastic model described in Section 2. The calculated displacements are passed onto the VUMAT subroutine as an input. The subroutine then uses those displacements to calculate the stress and plastic strain increments, assuming that the symmetric part of the total strain increment is additively decomposed into an elastic and plastic part. The response of the elastic–viscoplastic material is calculated assuming small-strain linear elastic deformations and Von Mises isotropic plasticity. Since our model contains two internal variables which are strain-dependent, an iterative scheme is used to update those internal variables and the plastic strain increment for each time step (Lush et al., 1989). Next, the calculated stresses are transferred back to the ABAQUS solver, which in turn uses them to find the displacements at the next time step, and so on. The deformations calculated with our model are not limited to small deformations, as this is taken care of by the ABAQUS solver itself when using the VUMAT subroutine through the use of the Green-Naghdi formulation (ABAQUS\Explicit, 2009b).

The specimen geometry considered in this study is the SCS (Rittel et al., 2002), which is a cylinder with two opposite grooves at 45° with respect to the longitudinal direction of the cylinder. This unique geometry enforces a state of dominant shear in the gauge section of the specimen (Dorogoy and Rittel, 2005), while a mild stress concentration exists in the fillets of the grooves, thus dictating the preferential locus for shear band formation. The SCS dimensions are 10 mm in diameter, gauge thickness of 2.5 mm and gauge width of 2 mm. The boundary conditions used for the simulations presented in the sequel are constant speed of 25 (m/s) on the upper surface of the specimen in the Z direction, and 0 displacement in the Z direction on the lower surface (see Fig. 2). These boundary conditions were chosen to replicate an experimental strain rate of 7000 (s^{-1}).

Special care was given to the element size inside the gauge since the simulation is a grain-scale one, meaning that each element is considered as a representative volume element (RVE) of a single material grain. Two element sizes (100 μm and 50 μm), as well as two element types (tetrahedral C3D4 and hexahedral C3D8R elements), were considered to check for convergence of the solution. All the macroscopic properties (averaged stress–strain curve, averaged strain rate and strain) were observed to be converged for the four mentioned possibilities. Convergence was also checked for local (element) properties. Here, values such as maximum and minimum local temperature, strain, strain rate and energy were compared and all found to be converged as well for the above-mentioned element types and sizes.

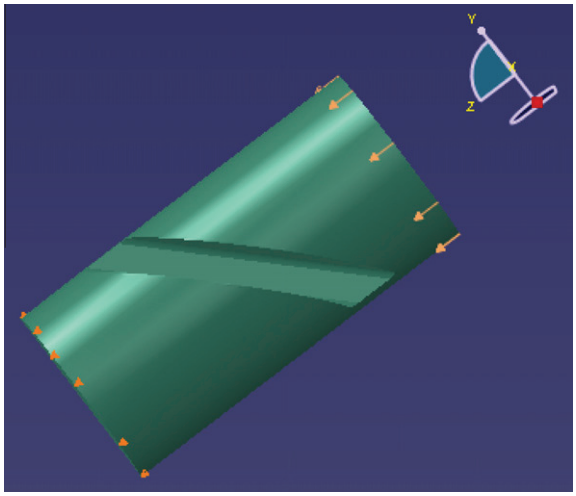

Fig. 2. The boundary condition used in the simulation shown on the SCS specimen.

The results presented in this work are those obtained for a gauge region meshed by 33600 C3D4 elements with an average element size of 100 μm (Fig. 2). Note that this value is the same as the averaged grain size of the tested material (pure Ti) on which the experimental values used in the model are calibrated.

Throughout this work, the calculated stresses and strains are the Mises equivalent ones, due to the three-dimensional stress condition prevailing in the gauge section (Rittel et al., 2002). Moreover, completion of the strain localization process will be assumed to be indicated by zero-hardening region of the stress–strain curve which precedes the final failure stage. This point will be identified here as the "failure strain".

4. Results

Numerical FEM simulations were carried out using the above-mentioned model and specimen geometry (SCS), to try and assess the respective role of temperature and microstructure evolution on the initiation of shear instabilities. The results will be presented in the following order:

4.1. Thermal softening

- First, a comparison will be held between three simulation in which no DRX is present ($U_{drx} \to \infty$), thus allowing us to study the sole effect of thermal softening by

changing the thermal softening parameter α in the range of $0–1 \times 10^{-3}$. Specifically, values of $\alpha = [0; 5e-4; 1e-3]$ were selected. Note that $\alpha = 5e-4$ corresponds to the averaged physically observed values of this coefficient (Chichili et al., 1998; Trojanova et al., 1994), while $\alpha = 1e-3$ is deliberately chosen to be quite high, in an attempt to simulate asymptotic thermal behavior.

- Next, the same values of α will be tested in the presence of DRX formation, in order to judge whether the thermal effects are still influential in the presence of microstructural evolution leading to potential additional softening.

4.2. Microstructural softening

The effect of microstructure will be determined by setting the thermal softening parameter α to be a constant, and varying the DRX threshold energy between the experimentally observed value – U^* (leading to DRX formation at $\varepsilon_p = 0.9\varepsilon_f^{exp}$, with ε_f^{exp} being the experimentally observed failure strain) and smaller values which correspond to materials in which DRX is observed at very early stages of the deformation (see e.g. Chichili et al., 1998; Trojanova et al., 1994 for the case of Ti–6Al–4V). Here, U^* (Eq. (7)) is calculated by multiplying the mechanical work invested in the process up to the first observed DRX at $\varepsilon = 0.9\varepsilon_f^{exp}$ by $(1-\beta)$, where β is the Taylor Quinney coefficient which was assumed to be 0.6, with σ_{flow}^{exp} being the experimentally measured flow stress.

$$U^* = (1-\beta)\int_0^{0.9\varepsilon_f^{exp}} \sigma_{flow}^{exp} d\varepsilon_p \tag{7}$$

The stress–strain response of each of the above mentioned test-cases will be analyzed to find the macroscopic (averaged) plastic strain at which the stress–strain curve becomes unstable, i.e. the strain hardening is becoming negative. This point will be defined as the "*failure strain*" of the model material (ε_f). Here it is important to emphasize that no failure model was implemented, and the term failure will be used to describe a loss in load bearing capability of the simulated specimens. This definition of the failure strain was discussed by Osovski et al. (2012) in the context of the spatial evolution of the DRX phase and resulting variations at the local vs. global strain rate. It was observed that the failure strain is achieved in parallel to the formation of a continuous band of DRX'ed elements at the fillet, furthermore it was shown that the local strain rate near a DRX'ed grain is up to 3 times higher than the average strain rate, thus indicating strong localization of the plastic strain.

4.3. Results on thermal effects

The stress–strain curve of a SCS-FEM model is presented for three different thermal softening parameters: $\alpha = [0; 5 \times 10^{-4}; 1 \times 10^{-3}]$, without considering DRX ($U_{DRX} = \infty$). As shown in Fig. 3, the resulting failure strains (arrowed) are $\varepsilon_f = [7.7; 1.15; 0.9]\varepsilon_f^{exp}$ respectively. Note that the maximum value used for α is clearly unphysical as it leads to negative Young's modulus at high temperatures, and as such represents an extreme case of thermal softening. Overall, the failure strain (point of instability) is seen to decrease with increasing α. Note that Fig. 4 represents the classically assumed scheme of thermal softening, supposed to lead to shear instability, in the absence of any other softening mechanism.

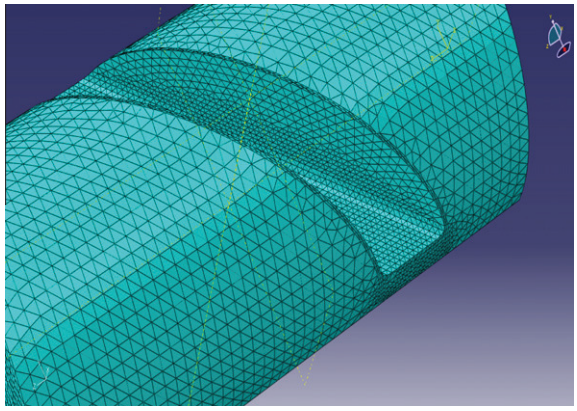

Fig. 3. SCS specimen with its gauge region meshed by 33600 C3D4 elements with an average element size of 100 μm.

Fig 5 presents a picture which is very much similar to that presented in Fig. 4, except for the fact that this time, the DRX threshold energy is now taken to be the experimentally observed value for pure Titanium, instead of infinity. This figure shows that, in comparison with Fig. 4, the range of failure strains shrinks significantly ($\varepsilon_f = [1.13; 1; 0.85]\varepsilon_f^{exp}$), as will be discussed in the sequel.

4.4. Results on microstructural softening effects

The role of microstructure with respect to temperature was studied by fixing $\alpha = 5 \times 10^{-4}$ and varying the energy required to initiate the appearance of DRX. In doing so, we

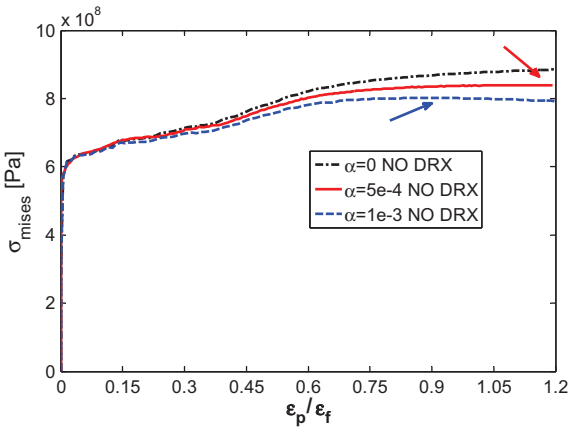

Fig. 4. Macroscopic equivalent stress–strain curves calculated for three different thermal softening parameters (α) *without DRX*. Note that when $\alpha = 0$, no strain-softening is predicted whereas increasing α values cause premature failure as indicated by arrows.

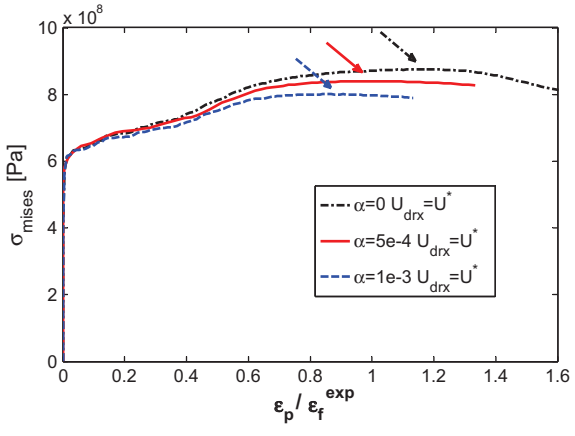

Fig. 5. Macroscopic equivalent stress–strain curves calculated for three different thermal softening parameters (α), all with the same DRX energy – U^*. Note that for a fixed microstructural parameter (U_{drx}), larger values of α lead to earlier specimen failure.

represent a material that exhibits very early DRX (e.g. Ti6Al4V) as opposed to e.g. pure Ti with its late DRX, close to final failure.

As shown in Fig. 6, it is obvious that the lower the relative energy for DRX (i.e. the earlier the DRX), the smaller the failure strain (arrowed), when all thermal effects are kept constant. In other words, early DRX favors early localized failure.

4.5. Results on microstructural softening effects – the role of latent heat

The results presented prior to this section were all obtained under the assumption that all of the energy stored during deformation is being released in the form of heat during the process of recrystallization ($f_{lh} = 1$). When comparing the above mentioned stress–strain curves with the ones calculated for the same sets of parameters but, under the assumption of no enthalpy release ($f_{lh} = 0$), the effect is almost negligible (see Fig 7), and the calculated failure strains for both cases appear to be almost identical. In other words, the additional heat produced by the release of latent heat produces has no noticeable macroscopic influence on the mechanical characteristics of the investigated material.

Let us now consider this issue on a more "microscopic", element scale. In Fig. 8, we have plotted the homologous temperature difference between the maximum and the average gauge temperatures, as a function of the normalized strain. One should note here that the hottest spot has a variable (element) location throughout the calculation.

In this comparison, the various parameters α, U_{drx}, f_{lh} are systematically varied to cover a wide range of possibilities. Several observations can be made from this figure. First of all, enthalpy release seems to contribute to a local temperature rise in the sense that it makes the hottest spot hotter. This is particularly evident in cases (a) and (b) where the thermal softening parameter α is lower. Here, higher temperatures will be reached when the energy level U_{drx} is greater and the fraction of recovered energy f_{lh} is larger. By contrast, when α is higher, as in cases (c) and (d), the release of enthalpy is seen to have quite a minor influence. Yet, a common feature to all the graphs is that up to normalized strains of about 0.6, the release of enthalpy has no appreciable effect. Moreover, considering only the cases where $f_{lh} = 1$, one notes that the strongest effect of enthalpy release is obtained for the smaller value of the thermal softening coefficient α a point to be addressed later.

4.6. On the development of hot spots

The notion of "hot-spot" has no rigorous definition, but is to be understood in the present context as a point where the local temperature exceeds significantly that of the surrounding medium. To address this issue, we present in Figs. 9–12 the thermal distribution in the gauge section, at different stages of the deformation for three sets of thermal and microstructural softening parameters, namely cases (a–c) of Fig. 8, and a 4th case, in which there is no

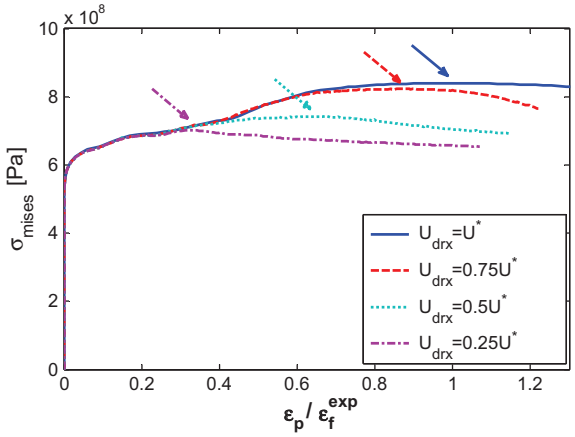

Fig. 6. Macroscopic equivalent stress–strain curves calculated for $\alpha = 5e-4$ and different DRX energies. Note that for a fixed thermal softening parameter (α), smaller values of DRX threshold energy promote earlier specimen failure.

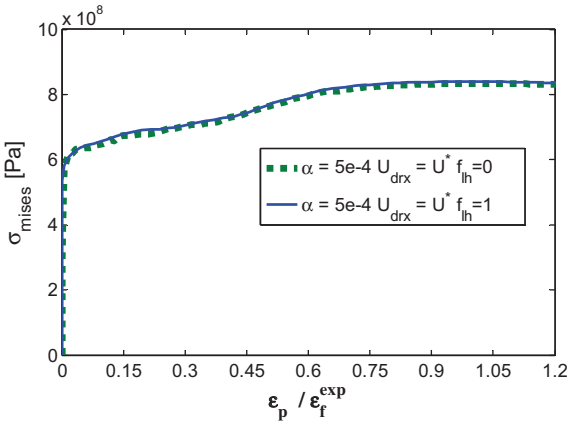

Fig. 7. Macroscopic equivalent stress–strain curves calculated for two values of f_{lh}. Note that the presence or absence of released enthalpy of recrystallization has almost no effect either on the average stress–strain characteristics, or on the failure strain.

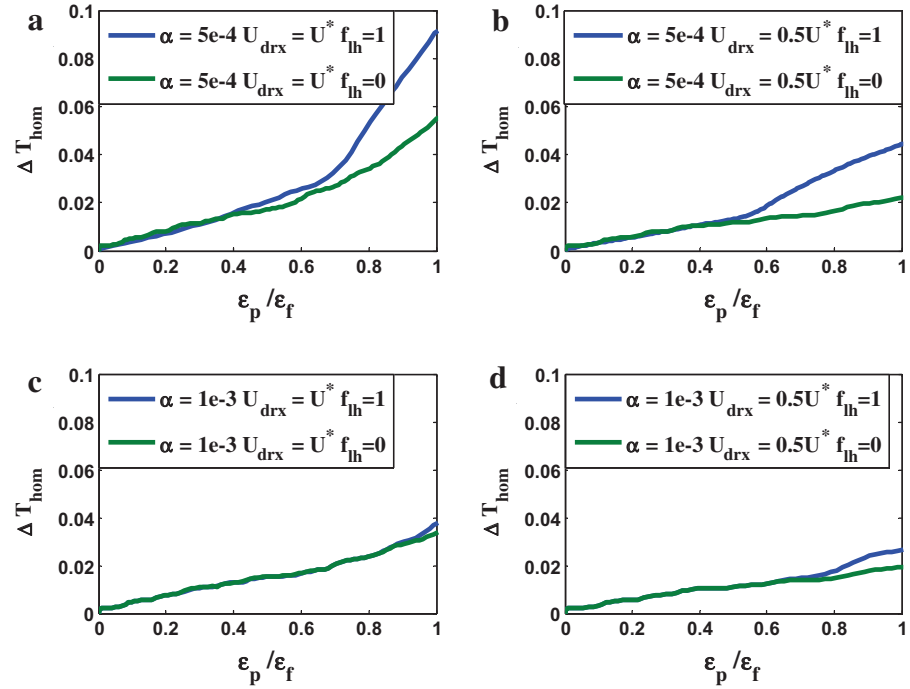

Fig. 8. The difference in homologous temperature between the averaged temperature in the gauge and the hottest spot in the gauge $\Delta T_{\text{hom}} = (T_{\max} - T_{\text{avg}})/T_{\text{melting}}$ is shown for four combinations of DRX energy (U_{drx}) and thermal softening coefficient (α). For each combination, the temperature difference is plotted for two values of f_{lh} accounting for total enthalpy release and no enthalpy release. Note that for $\alpha = 5e-4$ we get a much more significant effect than for $\alpha = 1e-3$, where the strong thermal softening limits the temperature increase.

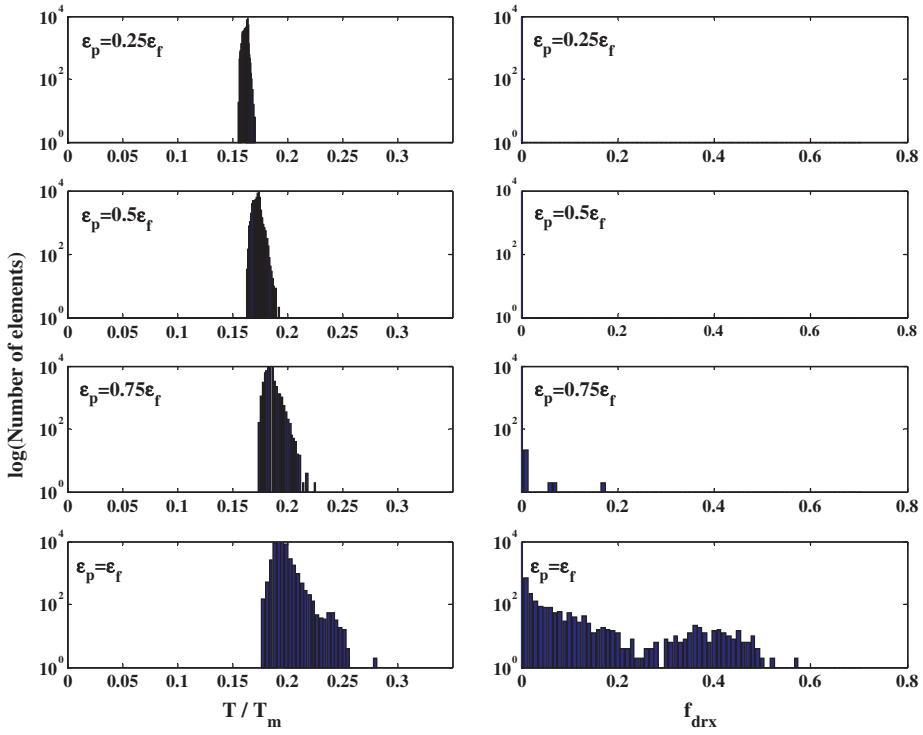

Fig. 9. Temperature and DRX volume fraction distributions at different stages of the deformation for $\alpha = 5e-4$ $U_{drx} = U^*$.

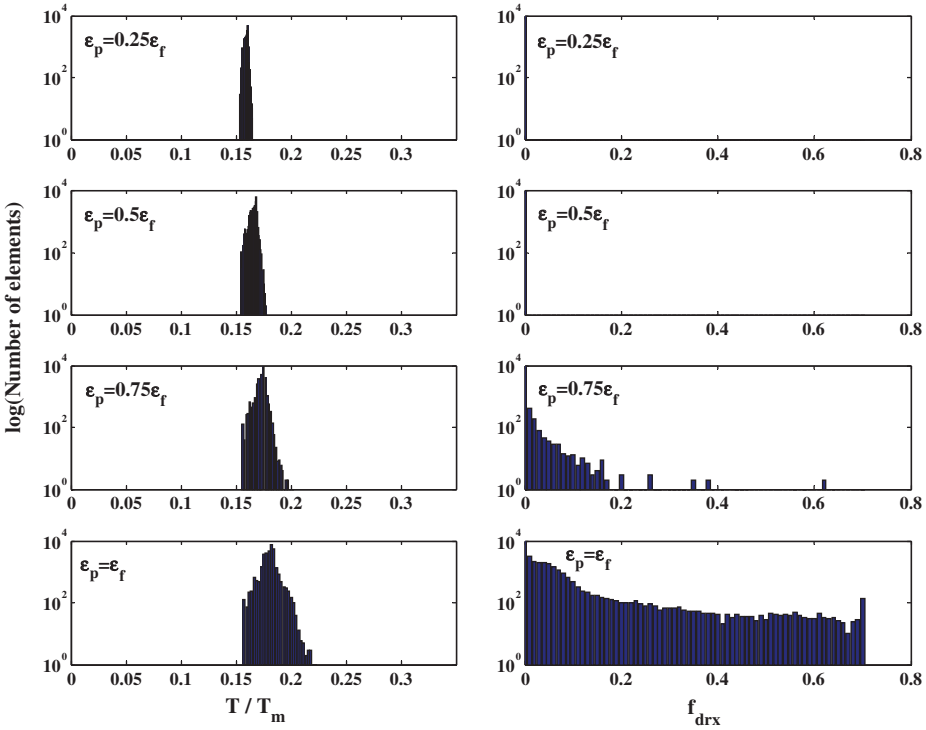

Fig. 10. Temperature and DRX volume fraction distributions at different stages of the deformation for $\alpha = 5e-4$ $U_{drx} = 0.5U^*$.

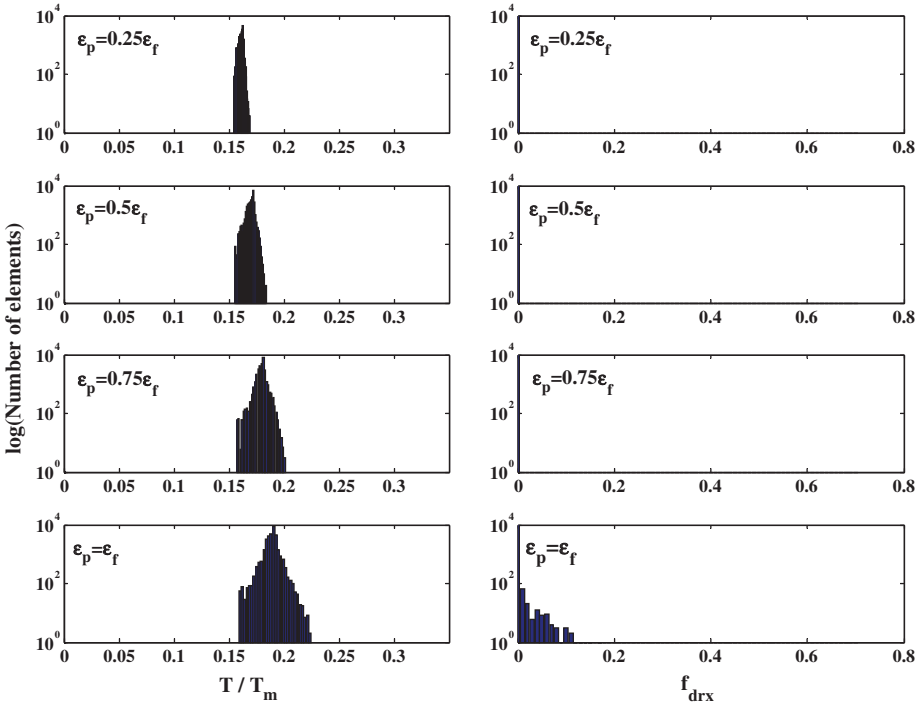

Fig. 11. Temperature and DRX volume fraction distributions at different stages of the deformation for $\alpha = 1e-3$ $U_{drx} = U^*$.

thermal softening ($\alpha = 0$), Fig 12. In parallel, we show the calculated evolution of the DRX volume fraction for each case.

A common feature to all the graphs is that the maximum homologous temperature does not exceed 0.35. In addition, one can note that as α increases for a given value

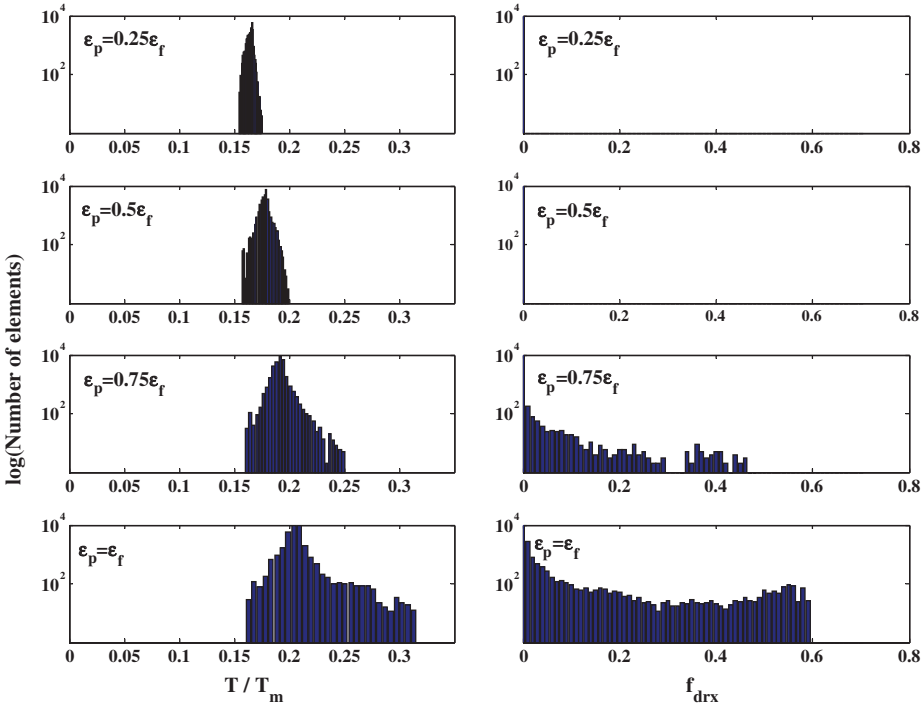

Fig. 12. Temperature and DRX volume fraction distributions at different stages of the deformation for $\alpha = 0$ $U_{drx} = U^*$.

of U_{drx}, the maximum (and average) temperatures in the gauge section decrease (Figs. 9, 11 and 12). Similarly, for a fixed value of α (Figs. 9 and 10), the largerU_{drx}, the higher the maximum (and average) temperatures reached in the gauge. Fig. 12 reveals the highest maximal temperatures in the gauge section. It also corresponds to a case without thermal softening and high U_{drx}. But these figures also clearly show that "hot-spots" formation, at best, accompanies DRX formation, instead of preceding it, as previously proposed. Consequently, these two phenomena are related, their extent depending on the thermo-physical properties of the material. However, Fig. 12 clearly shows that in order to observe hot spots, DRX needs to form at the later stages of the deformation and the thermal softening terms must be as small as possible. In other words, the material must have the capability to store large enough amounts of energy that will later be released as DRX and produce the observed hot spots.

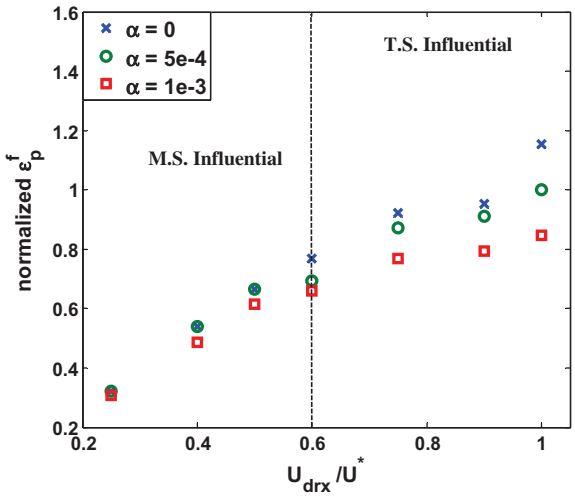

Fig. 13. Failure strains normalized to the experimentally observed value as a function of DRX energy threshold and thermal softening parameter. Two tentative regions can be observed (separated by the dashed line), one for which the thermal softening (T.S.) is more influential and a second region in which the microstructural softening (M.S.) becomes dominant.

The effective role of thermal and microstructural softening shown up to this point can now be summarized by plotting the normalized failure strain for different values of the thermal softening parameter and DRX threshold energy (Fig. 13). From this figure, it is seen that, while an increase in the thermal softening parameter can cause premature failure for materials with late DRX (e.g. $U_{drx}/U^* > 0.6$), when DRX starts at an earlier stage, thermal softening has little influence, if any. Consequently, this figure is divided into two distinct domains of influence for each softening mechanism.

5. Discussion

This works presents the results of a systematic investigation of the respective effects of thermomechanical coupling and microstructural evolutions on the onset of dynamic shear localization. We carried out several "numerical experiments" using a finite element representation of an experimental specimen, in which each element can undergo various microstructural and thermal evolu-

tions. The model is fully thermomechanically coupled under adiabatic assumptions. Thermal effects are represented by a thermal softening parameter α, as well as by the variable release (f_{lh}) of stored energy upon dynamic recrystallization.

The following discussion will focus on the main issues raised in the introduction, namely:

1. *What is the precise contribution of thermal softening, if at all, with respect to the above-mentioned microstructural softening.*

Several cases of thermal softening were examined, as summarized in Fig. 13 (see also Figs. 4 and 5). Our results show that thermal softening and microstructural evolutions cannot be entirely decoupled. If the microstructural evolution (DRX) occurs relatively early, e.g. $U_{drx}/U^* < 0.6$, the thermal softening factor has very little influence in the sense that it does not significantly affect the macroscopic failure strain. Here, the dominant factor is clearly the threshold energy at which DRX starts to develop, and the sooner it appears, the smaller the strain to failure of the material (Fig. 6). This would be the case of Ti6Al4V (Osovski et al., 2012) or Maraging steels for example. More generally, this is the general case of materials which fail at relatively low overall plastic strains with DRX appearing early during the deformation process, so that the thermal evolution is negligible. However, for those materials undergoing DRX at a later stage ($U_{drx}/U^* > 0.6$ in the present context), thermomechanical coupling effects will indeed affect the failure strain by reducing it. For the extreme case of a material that does not undergo DRX (e.g. pure Tantalum), the thermal softening factor is expected to play a dominant role, as illustrated in Fig. 4. Therefore, this work shows that thermal softening alone can eventually accelerate shear localization, provided that there are no microstructural evolutions like DRX, whose appearance precipitates failure before any significant thermal effects. Any intermediate situation between very early and no DRX formation at all can be interpolated from Fig. 13. To conclude this part of the discussion, the present work shows that both microstructural and thermal softening ought to be considered with special care paid to the chronology of these events.

1. *What is the contribution of the enthalpy release which is associated with the recrystallization process?*

From a macroscopic point of view, our results show that the release of enthalpy has no appreciable effect on the flow and failure characteristics of the material (Fig. 7). However, on a finer (element) scale, we observe that the enthalpy release affects the maximal temperature in the gauge section of the specimen, to an extent that is related to the physical properties of the investigated material (Fig. 8). Note also that in order to release enthalpy, a significant buildup of DRX in each element is required, so that the consequences of the release are only experienced after DRX has started to form. From Figs. 8 and 12, it is interesting to note the tendency towards increased thermal effects for the limiting case of no thermal softening at all, together with significantly delayed DRX formation ($U_{drx} = U^*$). While this result may seem strange at first sight, it just reflects the fact that when thermal softening is absent, the material can continue to store and dissipate higher levels of strain energy as long as microstructural softening is delayed. This would not be the case for a material that is weakened by strong thermal softening ($\alpha = 1e-3$) which overcomes the microstructural effects (down to $U_{drx} = 0.6U^*$ in this work).

1. *What is the contribution of hot spots, if any, on the onset of adiabatic shear failure?*

It has been postulated that thermal heterogeneities might be the cause leading to adiabatic shear instability, of the kind observed in granular explosives for instance. In this context, it is worth mentioning the work of Guduru et al. (2001) (Rittel et al. (2008) and Trojanova et al. (1994) who revealed experimentally that the thermal structure of an adiabatic shear band is far from being uniform, and that some hot spots with a well-defined thermal structure can be observed inside the band, once it was fully developed. The concept of a hot-spot is ill-defined in quantitative terms of what is considered as a significant thermal excursion from an average value. The series of histograms presented in Figs. 9 and 12 attempts to characterize the presence and extent of hot spots in the system, and indeed, one can find a small number of elements which form the right hand-side tail of the thermal distribution. However, a common feature of those figures is that one cannot really identify hotter spots at relative normalized strains of less than 0.75, while a well-developed tail is fully perceptible at failure, becoming really obvious for low to no thermal softening at all (Figs. 9 and 12). Yet, the important observation here is that "hot spots", if any, do not precede the formation of DRX phase, but rather come along with it.

The main tendency that appears from these histograms is that the stronger the softening mechanism, irrespective of its nature, the smaller the tendency to form hot-spots, and vice-versa (compare Figs. 9, 11 and 12, and separately with Figs. 9 and 10). In other words, "hot spots" are observed only for those cases where strain softening (either thermal and/or microstructural) is minimal. Here one should mention the analytical work of Molinari and Leroy (1991) who analyzed the thermal structure of a shear band using a perturbation analysis. One interesting outcome of this work was the observation that the structure is dictated by the ratio of thermal to strain-rate sensitivity (their β/m). Specifically, for small values of this term (of the order of 1), the structure becomes two-dimensional of the kind observed by Guduru et al. (2001). A direct numerical comparison is difficult since the thermal softening and the flow rule models of Molinari and Leroy (1991)) are slightly different from those used in this work. Yet, one can nevertheless observe that the β/m (similar to $= \alpha \cdot n$ in this work) ratio is certainly much smaller than unity. This corresponds to the two-dimensional modes reported by Molinari and Leroy (1991), albeit of a much smaller wavelength, which are regarded here as hot-spots. The comparison is all the more interesting that the approaches leading to similar results are very different (perturbation

analysis with thermal conduction vs. numerical adiabatic study).

Finally, our results point to the conclusion that the universally assumed positive feedback of thermal softening on heat generation becomes questionable. When a thermal softening mechanism is operative, it lowers the flow characteristics of a material, thereby impairing its capacity to dissipate (store) significant amounts of energy. Stated otherwise, the thermomechanical coupling, as seen in this work, appears to have a regulatory effect on the heat generation rather than providing a positive feedback, e.g. hot spots formation, leading to global instability of the material.

6. Conclusions

The main conclusions that can be drawn from this work are as follows:

1. Microstructural softening (DRX) plays a key role in dynamic shear localization. If present, it will override thermal softening effects.
2. The respective influence of thermal and microstructural softening is strongly dependent on the chronology of the two processes. Therefore, their influence cannot be completely decoupled, except for extreme cases such as Ta (thermal) and Ti6Al4V (microstructural).
3. The formation of "hot spots" should be understood as resulting from the localization process and not initiating it. In fact, hot spots will most likely tend to exist in materials undergoing DRX and minimal thermal softening.
4. The thermal softening mechanism plays a major role in stabilizing the thermal excursions in the material by lowering the rate of heat production, contrary to the common hypothesis of a positive feedback effect.
5. The present study is deemed to complete the physical picture, as to the relevant softening mechanisms and their domain of influence. As such, the results presented here do not question the generality of previous analytical work based on a general softening term, but rather emphasize the physical nature of this term.

Acknowledgement

The authors acknowledge Profs. A. Molinari and A. Needleman for many interesting discussions and suggestions. The support of the Israel Science Foundation (Grant 2011362) is gratefully acknowledged.

References

Abaqus\Explicit, 2009a. Abaqus Explicit v6.9 User's Manual. Dassault Systemes, Providence, RI.
Abaqus\Explicit, 2009b. Abaqus User Subroutines Reference Manual. Dassault Systemes, Providence, RI.
Avrami, M., 1939. Kinetics of phase change. I General theory. Journal of Chemical Physics 7, 1103.
Bai, Y., Dodd, B., 1992. Shear Localization: Occurrence, Theories, and Applications. Pergamon Press, Oxford, UK.
Bever, M., Holt, D., Titchener, A., 1973. The Stored Energy of Cold Work. Pergamon Press, London.
Bouaziz, O., Bréchet, Y., Estrin, Y., Embury, J.D., 2010. Critical grain size for dislocation storage and consequences for strain hardening of nanocrystalline materials. Scripta Materialia 63, 477.
Boyer, R., Welsch, G., Collings, E. (Eds.), 1994. Materials Properties Handbook: Titanium Alloys. ASM International.
Chichili, D.R., Ramesh, K.T., Hemker, K.J., 1998. The high-strain-rate response of alpha-titanium: experiments, deformation mechanisms and modeling. Acta Materialia 46, 1025.
Clayton, J.D., 2009. Modeling effects of crystalline microstructure, energy storage mechanisms and residual volume changes on penetration resistance of precipitate-hardened aluminum alloys. Composites: Part B 40, 443.
Dolinsky, M., Rittel, D., Dorogoy, A., 2010. Modeling adiabatic shear failure from energy considerations. Journal of the Mechanics and Physics of Solids 58, 1759.
Dorogoy, A., Rittel, D., 2005. Numerical validation of the shear compression specimen (SCS). Part II: dynamic large strain testing. Experimental Mechanics 45, 178.
Guduru, P.R., Rosakis, A.J., Ravichandran, G., 2001. Dynamic shear bands: an investigation using high speed optical and infrared diagnostics. Mechanics of Materials 33, 371.
Hill, W., Shimmin, K., 1961. Elevated temperature dynamic elastic moduli of various metallic materials, Wright Air Development Division Technical report 60–438.
Hosford, W., 2005. Mechanical Behavior of Materials. Cambridge University Press.
Jia, D., Wang, M., Ramesh, K.T., Zhu, T., Valiev, R.Z., 2001. Deformation behavior and plastic instabilities of ultra ne-grained titanium. Applied Physics Letters 79, 611.
Lush, A.M., Weber, G., Anand, L., 1989. An implicit time-integration procedure for a set of internal variable constitutive equations for isotropic elasto-viscoplasticity. International Journal of Plasticity 5, 521.
Medyanik, S., Liu, W., Li, S., 2007. On criteria for adiabatic shear band propagation. Journal of the Mechanics and Physics of Solids 55, 1439.
Molinari, A., Clifton, R.J., 1987. Analytical characterization of the shear localization in thermoviscoplastic materials. Journal of Applied Mechanics 54, 806.
Molinari, A., Leroy, Y.M., 1991. Structures in shear zones due to thermal effects. Comptes rendus de l'Académie des sciences 313 (Series II), 7.
Osovski, S., Rittel, D., Landau, P., Venkert, A., 2012. Microstructural effects on adiabatic shear band formation. Scripta Materialia 66, 9.
Padilla, H.A., Smith, C.D., Lambros, J., Beaudoin, A.J., Robertson, I.M., 2007. Effects of deformation twinning on energy dissipation in high rate deformed zirconium. Metallurgical and Material Transactions A 38A, 2916.
Remy, L., 1978. Kinetics of f.c.c. deformation twinning and its relationship to stress–strain behaviour. Acta Metallurgica 26, 443.
Rittel, D., Wang, Z.G., 2008. Thermo-mechanical aspects of adiabatic shear failure of AM50 and Ti6Al4V alloys. Mechanics of Materials 40, 629.
Rittel, D., Lee, S., Ravichandran, G., 2002. A shear compression specimen for large strain testing. Experimental Mechanics 42, 58.
Rittel, D., Ravichandran, G., Venkert, A., 2006. The mechanical response of pure iron at high strain rates under dominant shear. Materials Science and Engineering A A432, 191.
Rittel, D., Landau, P., Venkert, A., 2008. Dynamic recrystallization as a potential cause for adiabatic shear failure. Physical Review Letters 101, 165501.
Schoenfeld, S., Kad, B.K., 2002. Texture effects on shear response in Ti–6Al–4V plates. International Journal of Plasticity 18, 461.
Taylor, G.I., Quinney, H., 1934. The latent energy remaining in a metal after cold working. Proceeding of the Royal Society of London 143, 307.
Trojanova, A., Maksimiyuk, P.A., Lukáč, P., 1994. Temperature dependence of Young's modulus of α-titanium polycrystals. Physica Status Solidi (A) 143, K75.
Wright, T., 2002. The Physics and Mathematics of Adiabatic Shear Bands. Cambridge University Press, Cambridge.
Zener, C., Hollomon, J.H., 1944. Effect of strain rate upon plastic flow of steel. Journal of Applied Physics 15, 22.